Estimating Tropical Cyclone Wind Structure and Intensity From Spaceborne Radiometer and Synthetic Aperture Radar

Biao Zhang, *Senior Member, IEEE*, Ziqiang Zhu, William Perrie, Jie Tang, and Jun A. Zhang, *Senior Member, IEEE*

***Abstract*—We present a relatively simple method to estimate tropical cyclone (TC) surface wind structure (34-, 50-, and 64-kt wind radii) and intensity [maximum wind speed (MWS)] from wind fields acquired from the *L*-band SMAP radiometer and *C*-band Sentinel-1A/B and RADARSAT-2 synthetic aperture radar (SAR) between 2015 and 2020. The radiometer and SAR-derived wind radii and MWS are systematically compared with the best-track estimates. The root-mean-square errors (RMSEs) of R34, R50, and R64 are 31.2, 21.8, and 17.0 nmi (1 nmi = 1.852 km) for radiometer, and 21.7, 16.5, and 16.3 nmi for SAR, respectively. These error values are smaller than the averaged best-track uncertainty estimates for the three wind radii. Compared with the best-track reports, the bias and RMSE for the MWS estimates are −0.2 m/s and 5.8 m/s for radiometer, and 4.4 m/s and 9.1 m/s for SAR, respectively. These results are for the wind speeds in the range of 17–80 m/s. For the two typical TCs (Lionrock and Noru) in the Northwest Pacific Ocean, our results show that a combination of the radiometer and SAR wind data acquired within a very short time interval has the potential to simultaneously obtain reasonable measurements of the wind radii and intensity parameters. Moreover, for a TC with a long lifecycle, such as Typhoon Noru, we demonstrate that the high-resolution and multitemporal synergistic observations from SAR and radiometer are valuable for studying fine-scale features of the wind field and characteristics of wind asymmetry associated with intensity change, as well as the evolution of TC surface wind structure and intensity.**

***Index Terms*—Intensity, radiometer, synthetic aperture radar (SAR), tropical cyclone (TC), wind structure.**

Manuscript received December 8, 2020; revised February 14, 2021; accepted March 9, 2021. Date of publication March 17, 2021; date of current version April 21, 2021. This work was supported in part by the Joint Project between National Science Foundation of China and Russian Science Foundation under Grant 42061134016, in part by the National Science Foundation of China under Grant 42076181, in part by Shanghai Typhoon Foundation under Grant TFJJ201902, in part by the International Cooperation Project of the National Natural Science Foundation of China under Grant 41620104003, in part by European Space Agency–Ministry of Science and Technology China Dragon-5 Programme under Grant 58290, in part by the Government Research Initiative Program of the Canadian Space Agency, and in part by the Ocean Frontier Institute of Dalhousie University, Fisheries and Oceans Canada Surface Water and Ocean Topography program. The work of Jun A. Zhang was supported in part by National Oceanic and Atmospheric Administration under Grant NA14NWS4680028 and in part by National Science Foundation under Grant AGS1822128. *(Corresponding author: Biao Zhang.)*

Biao Zhang is with the School of Marine Sciences, Nanjing University of Information Science and Technology, Nanjing 210044, China, and also with the Southern Marine Science and Engineering Guangdong Laboratory (Zhuhai), Zhuhai 519080, China (e-mail: zhangbiao@nuist.edu.cn).

Ziqiang Zhu is with the School of Marine Sciences, Nanjing University of Information Science and Technology, Nanjing 210044, China (e-mail: ziqiang_zhu@nuist.edu.cn).

William Perrie is with the Department of Fisheries and Oceans Canada, Bedford Institute of Oceanography, Dartmouth, NS B2Y 4A2, Canada (e-mail: William.Perrie@dfo-mpo.gc.ca).

Jie Tang is with the Shanghai Typhoon Institute, China Meteorological Administration, Shanghai 200030, China (e-mail: tangj@typhoon.org.cn).

Jun A. Zhang is with the Hurricane Research Division, Atlantic Oceanographic and Meteorological Laboratory, National Oceanic and Atmospheric Administration, Washington, DC 20230 USA, and also with the Cooperative Institute for Marine and Atmospheric Studies, University of Miami, Miami, FL 33149 USA (e-mail: jun.zhang@noaa.gov).

Digital Object Identifier 10.1109/JSTARS.2021.3065866

I. Introduction

TROPICAL cyclone (TC) surface wind structure includes the maximum extents for three important indicators of wind intensity, namely gale-force winds (34 kt), destructive winds (50 kt), and hurricane-force winds (64 kt), as measured radially in the four geographic quadrants of a storm. Here, 1 kt = 0.514 m/s. These wind radii are important for TC readiness assessment [1]. The operational wind radii estimates are used to provide TC wind speed probabilities for early risk warnings and precautions [2]. The objective specification of TC wind radii is also utilized to initialize numerical weather prediction models, and its accuracy can have a significant positive impact on TC intensity forecasts, especially for rapid TC intensification [3]. TC intensity is typically defined as 1 or 10-min maximum sustained wind speed at a 10-m reference observing level [4], which is one of the metrics used to estimate potential wind destruction [5]. Thus, for TC forecast purposes, it is very important to determine the surface wind structure.

Satellite remote sensing observations have been used to estimate TC intensity and wind structure, either using the original satellite data or resulting derived wind fields. A pioneer method to subjectively estimate TC intensity is called the Dvorak technique, which is based on the analysis of cloud characteristics of visible images from geostationary meteorological satellites [6]. This approach has been further improved for objectiveness and automation purposes [7], [8]. In addition to intensity estimates, geostationary satellite infrared images and model analyses have been used for estimating TC wind radii parameters [9], [10]. TC intensity and surface wind structure can be simultaneously estimated using observed advanced microwave sounding unit data

from meteorological satellites based on a multiple-regression method [11], or from the cyclone global navigation satellite system wind speed observations using a parametric wind profile model [12]. *Ku*-band satellite scatterometer winds have also been used for estimating TC intensity, but the rain attenuation and signal saturation can lead to a large negative bias in intensity estimates [13]. Scatterometer winds, however, are useful for TC outer-core wind analyses [14], [15], especially for the 34-kt wind radii estimation [16].

Spaceborne *L*-band radiometers are excellent passive microwave sensors for remotely measuring the wind speed in TCs because the wind-induced brightness temperature is sensitive to high wind speeds and does not show any apparent sign of saturation [17]–[19]. Compared with *Ku*-band scatterometers, *L*-band radiometers onboard soil moisture ocean salinity and the soil moisture active/passive (SMAP) satellites are much less susceptible to the rain attenuation. Rain-induced scattering can be nearly ignored because the electromagnetic wavelength of the *L*-band is much larger than the size of rain droplets. Due to these advantages, *L*-band radiometers can provide the accurate measurements of high winds with large coverage under extreme weather conditions and, thus, provide the estimates of TC size [20], [21]. Statistical comparisons between the SMAP-derived wind speeds and SFMR measurements, from eight TCs during 2015, have shown that the standard deviation of wind speed was 3.11 m/s for wind speeds up to 70 m/s [19]. Moreover, as an application, SMAP wind data acquired in the Northwest Pacific Ocean have been used to examine TC surface wind asymmetry [22].

Compared with radiometers, spaceborne synthetic aperture radars (SARs) have higher spatial resolutions and, thus, can provide fine-scale structural features in the TC surface wind fields. *C*-band cross-polarized SAR signals have been shown to be sensitive to wind speeds but not sensitive to incidence angles or wind directions under high wind conditions [23]. Studies have shown that the *C*-band co- and cross-polarized SAR observations can be used to retrieve the accurate TC wind fields [24]–[27]; the root-mean-square error (RMSE) is about 5 m/s for wind speeds up to 75 m/s compared with the collocated SFMR observations [27]. Moreover, TC centers, radii of maximum wind speed, and the azimuthal wavenumber one asymmetry of surface winds have been studied using the cross-polarized SAR images [28]. A recent study has shown that SAR-derived high-resolution TC wind fields can be used to estimate the parameters related to TC wind structure [27].

In this study, for the first time, we use both spaceborne radiometer and SAR wind fields to estimate TC surface wind radii and intensity, and systematically evaluate the associated errors against the international best-track archive for climate stewardship (IBTrACS) data. The synergistic wind field observations from SAR and radiometer are used to exhibit the evolution of TC intensity and structure. The remaining part of this article is organized as follows. The dataset is described in Section II. The methodology and results are presented in Section III. Finally, Section IV presents the conclusion of this article.

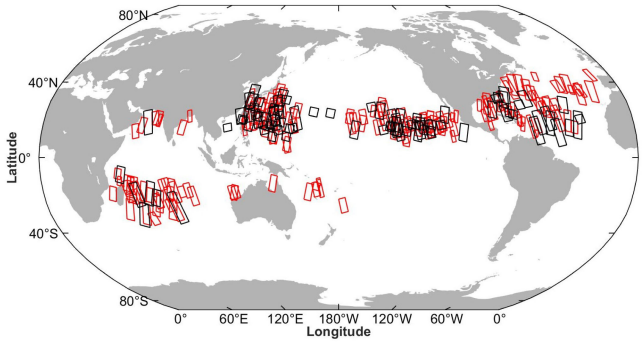

Fig. 1. Geographic locations of SAR images of 118 TCs. The red and black squares denote S1-A/B and RS-2, respectively.

II. Dataset

A. SMAP Radiometer TC Winds

The SMAP satellite was originally designed to measure soil moisture by using a combination of observations from a radiometer and a SAR. The near-polar orbit of SMAP allows for complete global coverage of the oceans over 3 days with a repeat cycle of 8 days. The spatial resolution and the coverage of the radiometer are about 40 km and 1000 km, respectively. In addition to the soil moisture measurement, the *L*-band radiometer onboard SMAP has been demonstrated to be an excellent microwave instrument for high wind observations, even in heavy precipitation conditions, such as TCs [18]. SMAP wind data with a spatial resolution of $0.25° \times 0.25°$ may be publicly obtained through the remote sensing systems website (www.remss.com/missions/smap/). In order to estimate TC wind structure and intensity, SMAP *L*-band radiometer-measured surface wind fields from 257 TCs were acquired over the West Pacific, East Pacific, Atlantic, and South Indian basins between April 2015 and December 2019.

B. Sentinel-1 and RADARSAT-2 SAR TC Winds

As a part of the Canadian Space Agency hurricane watch program and European Space Agency satellite hurricane and observation campaign, a total of 118 TCs were observed by *C*-band RADARSAT-2 (RS-2) and Sentinel-1A/B (S1-A/B) dual-polarization (VV+VH) SAR, over the North Atlantic, Northeast Pacific, Northwest Pacific, South Pacific, and Indian Oceans between May 2015 and October 2020. Fig. 1 shows the geographic locations of the TC SAR images. The imaging modes are interferometric wide (IW) and extended wide (EW) for S1-A/B and ScanSAR wide for RS-2, respectively. The swath width for the IW and EW modes is 250 km and 400 km, respectively; for the ScanSAR wide mode, the swath is 500 km. The incidence angles range from 17° to 49° depending on the sensor and/or modes. For S1-A/B, the spatial resolutions in the range and azimuth directions for the IW and EW modes are 5×20 m and 20×40 m, respectively; and for the RS-2 ScanSAR wide mode, these are 163×73 m and 78×106 m. Studies have shown that dual-polarization SAR data can be used to retrieve high-resolution TC wind speeds and directions [24]–[27]. In

this study, the ocean surface wind fields with a 3 km resolution derived from S1-A/B and RS-2 dual-polarization SAR images are used to estimate TC wind radii and maximum wind speed.

C. TC Best-Track Data

TC best-track data were obtained from the IBTrACS dataset (the USA subsets), which combines TC track and intensity, as well as structural estimates from currently available best-track data from multiple agencies. IBTrACS provides a central repository of TC track data [29], which consists of the best estimates of the TC central position (latitude and longitude), central pressure, storm intensity (1-min maximum sustained wind), and structure parameters, such as the 34-, 50-, and 64-kt wind radii, at 6-h intervals. The best-track data have been widely used to validate the model predictions of TC track and intensity [30] to investigate TC intensification trends [31],[32], to analyze the global variation of TC translational speed [33], and changes in the life circles of major TCs with time [34]. All the best-track data in this study are from IBTrACS version 4.0.[1] TC wind radii and intensity parameters from the best-track database are compared with SMAP radiometer and SAR estimates.

III. Methodology and Results

A. TC Wind Radii and Intensity Estimation Method

To estimate TC surface wind structure and intensity parameters, we interpolate the IBTrACS best-track data to the time of SMAP radiometer, S1-A/B and RS-2 SAR observations in order to determine the location of a given TC center, for each observation. TC wind fields from radiometer and SAR observations are used to extract the maximum wind speed ($V_{\max}$) and 34-, 50-, and 64-kt wind radii in four earth-relative quadrants. The method for estimating TC wind radii and $V_{\max}$ can be summarized as three steps. *First*, the contours of each wind radii are computed, which consists of a number of line segments. *Then*, we calculate the distances from the TC center to each point of the longest line segment in each quadrant. *Finally*, the 90% cumulative distribution of this distance is defined as the wind radii of a given wind threshold at that quadrant. Hereafter, the 34-, 50-, and 64-kt wind radii are referred to as R34, R50, and R64, respectively. Fig. 2 shows the flowchart for estimating the TC surface wind structure and intensity using the spaceborne radiometer and SAR data. As an example, Fig. 3 illustrates the estimates of R34 and $V_{\max}$ for Typhoon Noru using SMAP wind observations acquired in the Northwest Pacific at 21:19 UTC on August 1, 2017. For this case, $V_{\max}$ from the SMAP data and best-track data is 41.5 m/s and 46.3 m/s, respectively. The red and purple solid lines stand for R34 from the best-track and SMAP data, respectively. The SMAP-estimated R34 is 119.9 nmi, 107.5 nmi, 103.1 nmi, and 112.3 nmi in the northeast (NE), southeast (SE), southwest (SW), and northwest (NW) quadrants, respectively; these are consistent with the corresponding best-track estimates of 125.0, 124.5, 112.2, and 120.0 n mi.

[1]Online. [Available]: https://www.ncdc.noaa.gov/ibtracs/

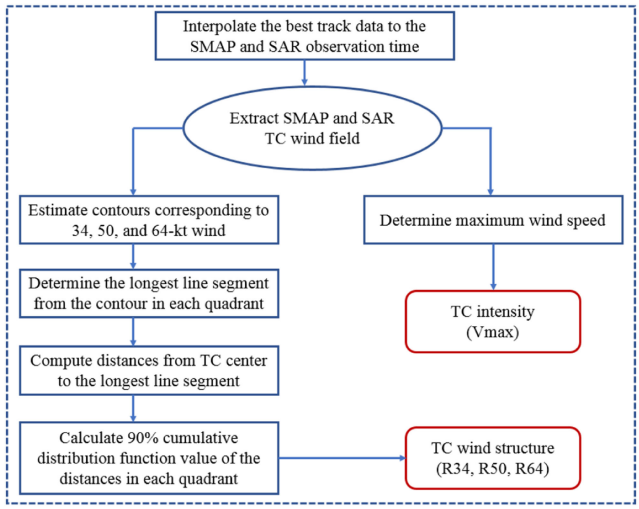

Fig. 2. Flowchart for estimating TC surface wind structure (R34, R50, and R64) and intensity ($V_{\max}$) from spaceborne radiometer and SAR wind data.

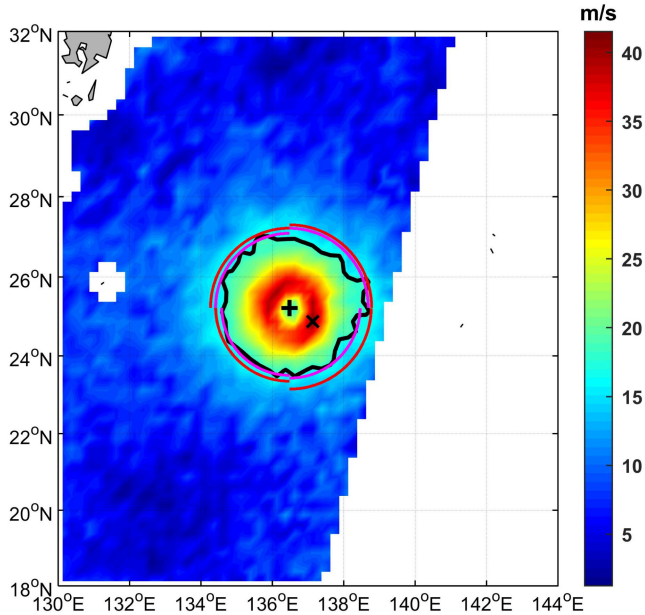

Fig. 3. SMAP wind field and estimated 34-kt wind radii (R34) of Typhoon Noru in Northwest Pacific at 21:19 UTC on August 1, 2017. The black plus and cross represent the locations of the typhoon center and maximum wind speed ($V_{\max}$), respectively. The black solid line denotes the contour corresponding to the 34-kt wind. The red and purple solid lines stand for wind radii at 34 kt from the IBTrACS best-track data and from SMAP winds.

B. TC Wind Radii and Intensity Validation

Based on the method described in Section III-A, we analyzed all SMAP wind data to calculate TC surface wind parameters and compared the results with the best-track data. As shown in Fig. 4(a)–(c), the RMSEs of R34, R50, and R64 are 31.2 nmi (57.8 km), 21.8 nmi (40.4 km), and 17.0 nmi (31.6 km), respectively. Note that these values are smaller than those from previously reported best-track uncertainties of 39.8 nmi, 32.3 nmi, and 24.4 nmi for R34, R50, and R64, respectively [35].

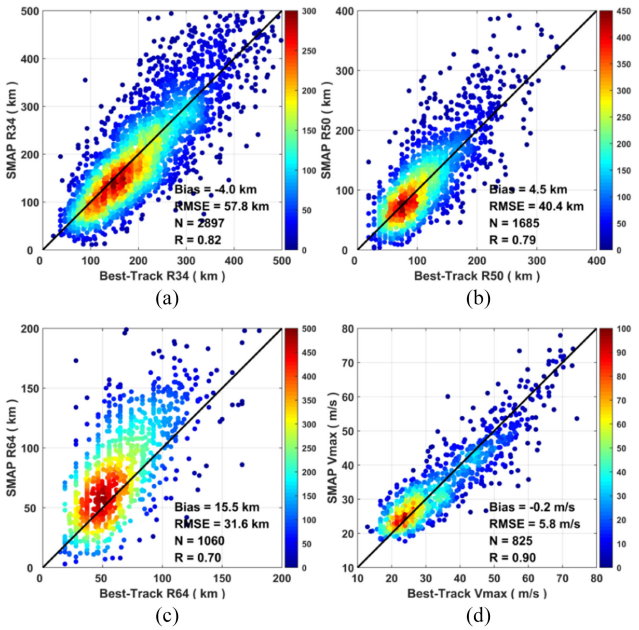

Fig. 4. Statistical comparison of wind radii (R34, R50, and R64) and maximum wind speeds ($V_{\max}$) between the best-track and SMAP data. The black diagonal lines represent one-to-one reference. The colorbars represent the number of data points in the specific bins. The bin size is 50 × 50 km for (a)–(c) and 5 × 5 m/s for (d). Each colored point is located at the center of the bin.

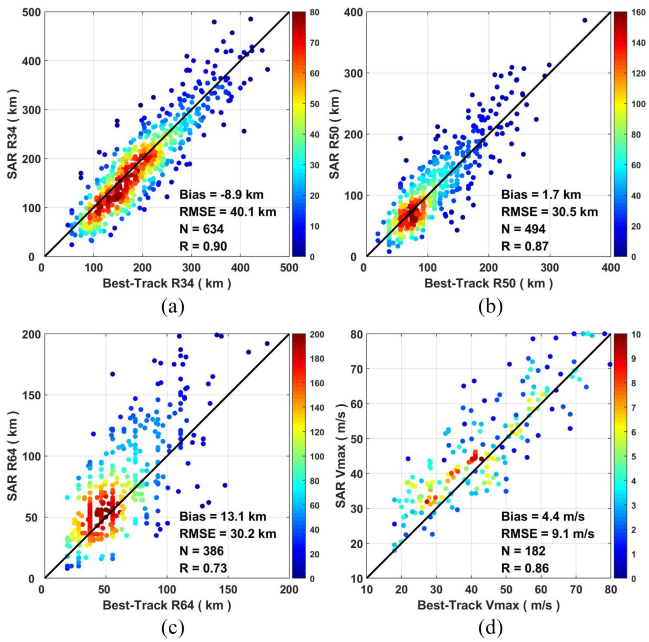

Fig. 5. Statistical comparison of wind radii (R34, R50, and R64) and maximum wind speeds ($V_{\max}$) between the best-track and SAR (S1-1A/B and RS-2) data. The black diagonal lines represent one-to-one reference. The colorbars represent the number of data points in the specific bins. The bin size is 50 × 50 km for (a)–(c) and 5 × 5 m/s for (d). Each colored point is located at the center of the bin.

The correlation coefficients between the SMAP-estimated wind radii and the best-track data are in the range of 0.70–0.82. The biases of SMAP-estimated R34, R50, and R64 are −2.1 nmi (−4.0 km), 2.4 nmi (4.5 km), and 8.3 nmi (15.5 km), respectively. We also compare $V_{\max}$ derived from the SMAP wind fields with those from the best-track reports [see Fig. 4(d)]. To make the comparison more meaningful, following the article presented in [19], we transformed the 1-min sustained $V_{\max}$ into 10-min sustained $V_{\max}$ using the scale factor of 0.93, as recommended by the World Meteorological Organization [4]. A high correlation of 0.9 between the SMAP-estimated $V_{\max}$ and the best-track data is found. The bias and RMSE of the SMAP estimates are −0.2 m/s and 5.8 m/s, respectively.

Note that SMAP is a near-polar orbiting satellite such that its passes are infrequent (on the order of one or two every day) in the low and middle latitude regions. Thus, only a portion of TC is usually observed by SMAP. Under these circumstances, not all wind radii in four geographic quadrants can be estimated using SMAP wind data. Moreover, the best-track R64 estimates are computed via a linear regression from the R34 values (e.g., West Pacific).[2] It should be noted that the TC best-track wind radii estimation relies heavily on the satellite data, particularly scatterometer measurements (e.g., QuikSCAT) when *in situ* observations and aircraft measurements are not available. However, *Ku*-band QuikSCAT winds are significantly affected by the rain attenuation and instrumental signal saturation under storm-force wind conditions [13], which can result in large uncertainty in the wind radii estimates. These factors may be the reasons for the discrepancy between the SMAP estimates and best-track reports, especially for R64 estimates.

We extract $V_{\max}$ from SMAP gridded wind data with a spatial resolution of 0.25° × 0.25°. This product is obtained from instantaneous 40 km spatial averages of the SMAP observations. For very strong TCs with small eyes (<20 km), SMAP cannot resolve the TC eyes due to its coarse resolution. Accordingly, the spatial average in the eyewall regions of small storms can cause the underestimation of $V_{\max}$. Moreover, the best-track $V_{\max}$ estimates have the average uncertainties of about 10.6 kt (5.5 m/s), even when satellite and aircraft measurements are both available for major hurricanes [35], [36]. The effects of SMAP spatial averaging and inherent uncertainties of the best-track data possibly account for the negative bias of $V_{\max}$ between the SMAP and best track.

Compared with the *L*-band SMAP radiometer, *C*-band SAR satellites (S1-A/B and RS-2) have much higher spatial resolutions. Here, we use S1-A/B and RS-2 high-resolution TC wind fields to estimate R34, R50, and R64, and compare them with the best-track data. The results are shown in Fig. 5(a)–(c). The RMSEs of SAR-estimated R34, R50, and R64 are 21.7 nmi (40.1 km), 16.5 nmi (30.5 km), and 16.3 nmi (30.2 km), respectively. Similar to the SMAP result, these errors are smaller than the corresponding values of wind radii uncertainty from the best-track data for major hurricanes. Furthermore, there is a good correlation between the SAR and best-track wind radii with the correlation coefficients of 0.90 for R34, 0.87 for R50, and 0.73 for R64. In addition to the wind radii, we also compare best-track estimates for 1-min sustained $V_{\max}$ with those extracted from SAR wind fields. Compared with SMAP,

[2]Online. [Available]: https://www.metoc.navy.mil/jtwc/jtwc.html?western-pacific

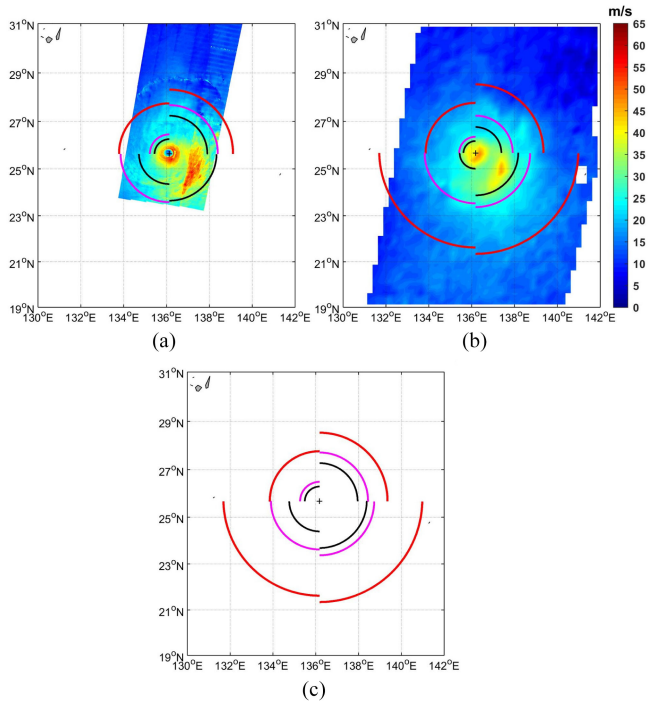

Fig. 6. Wind fields and wind radii (R34, R50, and R64) of Typhoon Lionrock from (a) S-1A and (b) SMAP. (c) Composite wind radii from SAR and SMAP. The red, purple, and black solid lines stand for the estimated R34, R50, and R64, respectively. The location of the TC center is illustrated by a black plus.

the spatial resolution of SAR-derived winds is much higher, and thus, we do not need to do a scaling operation on $V_{\max}$ from the best-track data. As shown in Fig. 5(d), two estimates are strongly correlated, with a correlation coefficient of 0.86. The bias and RMSE of SAR-measured $V_{\max}$ are 4.4 m/s and 9.1 m/s, respectively, compared with the best-track data.

The weak TCs with very large sizes cannot be fully observed by SAR because of its limited spatial coverage (250–500 km), which may result in larger RMSE error in R34 estimates than in other wind radii. A positive bias in the SAR-measured values for $V_{\max}$ is expected because SAR measures the instantaneous wind, while the best-track estimates for $V_{\max}$ are based on the measurements of the 1-min maximum sustained wind speed. Moreover, rain effects on the *C*-band SAR signals under high wind conditions may contribute to relatively large scatter in the SAR-derived wind speeds, which can result in relatively large RMSE. The average uncertainty in the best-track $V_{\max}$ is about 13.5 kt (6.9 m/s) for major hurricanes when only the satellite measurements are available [35], which is also a contributing factor for the large RMSE.

Fig. 6 shows the SMAP radiometer and S1-A SAR wind fields of Typhoon Lionrock in the Northwest Pacific. The time interval between SMAP and S1-A is only 16 min. This provides a good opportunity to estimate $V_{\max}$ and wind radii using wind field observations from different spaceborne microwave sensors. The translational speed of Typhoon Lionrock at SMAP and S1-A acquisition was 6.9 m/s and this storm moved 6.6 km in such a short time span. As shown in Fig. 6(a), the S1-A-derived wind field clearly illustrates the typhoon eye and fine-scale structure features. By contrast, Fig. 6(b) shows that SMAP does not resolve the typhoon eye, owing to its coarse resolution. To note, SMAP and S1-A both show an asymmetric wind distribution. The S1-A- and SMAP-derived $V_{\max}$ are 62.6 m/s and 48.1 m/s, respectively. According to the best-track report, the $V_{\max}$ is 60.6 m/s. Apparently, SMAP underestimates $V_{\max}$, likely due to the effect of spatial averaging. R64 estimates from SMAP and S1-A are close in the NW quadrant, giving 30.2 nmi (56.0 km) and 37.3 nmi (69.0 km), respectively. In this quadrant, the best-track R64 is 41.5 nmi (76.9 km) supporting the S1-A estimate. However, notable R64 differences between these two satellite estimates and the best-track report are found in the other three quadrants. SMAP and S1-A R50 estimates are in good agreement in the SW quadrant, with the values of 123.1 nmi (228.0 km) and 128.5 nmi (238.0 km), respectively, which are much larger than the best-track data, with a value of 102.6 nmi (190 km). In the SE quadrant, R50 is absent in the S1-A estimate because of the limitation of the spatial coverage. R34 estimates from SMAP and S1-A in the NE and NW quadrants are close to each other and to the best-track data. However, S1-A cannot provide R34 measurement in the SW and SE quadrants due to swath issues.

Considering the very short time interval between the SMAP and S-1A measurements, it is possible to use the synergistic observations of these two satellites to obtain reasonable wind radii estimates in the four quadrants. Fig. 6(c) shows that the composite of the wind radii is a combination of SMAP-estimated R34 and S1-A-estimated R64 and R50 values. R50 in the SE quadrant is estimated from SMAP wind data. For the case of Typhoon Lionrock, S1-A can provide more accurate estimates for $V_{\max}$ than SMAP. Regarding wind radii estimates, SMAP is better than S1-A in estimating R34 because the former has larger coverage. However, SMAP-derived values for R50 and R64 may not be as good as those from S1-A due to the impact of spatial averaging. As a consequence, the accurate TC surface wind structure and intensity parameters are expected to be derived by using the combined observations from both the radiometer and SAR.

Typhoon Noru was a long-lived TC that lasted from July 19 to August 9, 2017, in the Northwest Pacific. During its lifetime, SMAP and RS-2 performed a total of 17 overpasses over the storm. Here, we present 12 of these overpasses that have sufficient spatial coverage to estimate R34, at least in one quadrant of the storm at a given time. The evolution of the wind field from both SMAP and RS-2 measurements and the estimated R34 (black solid lines) during the lifecycle of Typhoon Noru are shown in Fig. 7, together with the best-track R34 (black-dotted lines). It appears that the R34 estimates from SMAP generally match well with the radial extents of gale-force winds reported by the best-track data. R34 estimates from the RS-2 and best-track data are comparable on July 29 and August 4 because the radial extents of gale-force winds are covered by the RS-2. However, notable differences between the RS-2 and the best-track-measured R34 are found on July 27 and 30 due to RS-2's swath limitation. For this case, the synergistic use of multitemporal wind fields from SMAP and RS-2 exhibits the evolution of intensity and the surface wind structure of Typhoon Noru. As shown in Fig. 7, Noru was a tropical storm on July

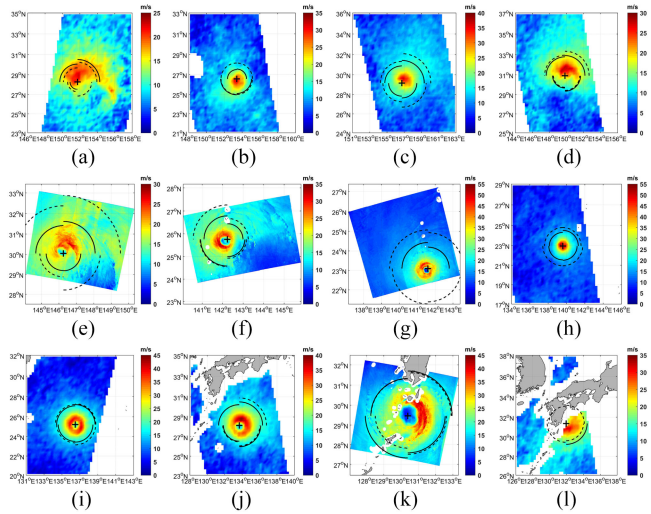

Fig. 7. Mosaic of successive wind fields derived from SMAP and SAR (RS-2) during the evolution of Typhoon Noru in the Northwest Pacific from July 22 to August 6, 2017. The location of the TC center is illustrated by a black plus. The black dotted and solid lines are 34-kt wind radii (R34) reported by best track and estimated from SMAP or SAR wind fields.

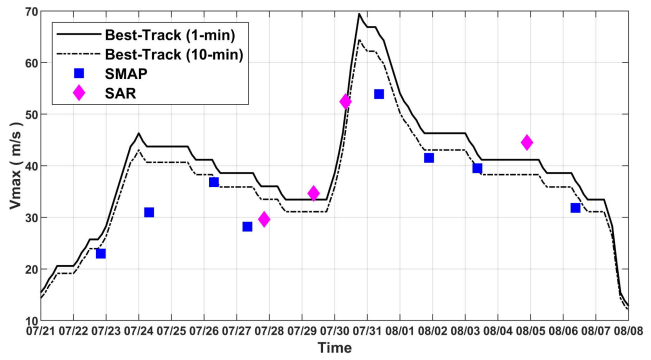

Fig. 8. Time series of best-track maximum 1-min (black solid line) or 10-min (black dash–dot line) sustained wind speed for Typhoon Noru from July 21 to August 8, 2017. Blue squares indicate SMAP peak winds. Cyan rhombi are RS-2 peak winds.

22, further intensified into a typhoon on July 24 and maintained this status until July 26. Thereafter, it weakened to a severe tropical storm again on July 27, and then rapidly intensified into a super typhoon with associated annular characteristics on July 31. In early August, Noru underwent a gradual weakening. After stalling off the southern part of Japan, it weakened again to a severe tropical storm on August 6. During the lifecycle of Typhoon Noru, SMAP and RS-2 both clearly show both symmetric and asymmetric distributions of the wind fields. When Noru is weak, the surface wind is asymmetric, whereas when the storm is strong, it is close to symmetric. Moreover, as shown in Fig. 8, SMAP- and RS-2-derived maximum wind speeds reveal the intensity change of Typhoon Noru during its lifecycle, which is consistent with the best-track report.

IV. Conclusion

In this study, the SMAP *L*-band radiometer wind field of 257 TCs and the *C*-band Sentinel-1A/B and RADARSAT-2 SAR wind fields of 118 TCs are acquired and collocated with the IBTrACS data. We estimated 34-, 50-, and 64-kt wind radii (R34, R50, and R64) and maximum wind speed ($V_{\max}$) using the SMAP- and SAR-measured TC wind fields based on a relatively simple method and compared them with the best-track data. The resulting RMSE values for R34, R50, and R64 are 31.2, 21.8, and 17.0 nmi for SMAP; and 21.7, 16.5, and 16.3 nmi for SAR, respectively. SMAP- and SAR-estimated maximum wind speeds are also compared with the best-track reports. The bias and RMSE are -0.2 m/s and 5.8 m/s for SMAP, and 4.4 m/s and 9.1 m/s for SAR, respectively. The discrepancies between the SMAP- and SAR-estimated wind radii and maximum wind speeds and those from the best-track data are possibly associated with spatial averaging and restrictions on the swath, the inherent uncertainty in the best-track data, and different intensity definitions for the satellite data and best-track data.

SMAP and SAR have their own strengths and weaknesses, regarding the measurement of TC surface wind fields, and estimates of wind radii and intensity parameters. The *L*-band SMAP radiometer signals are sensitive to high wind speeds and less affected by rain and, thus, can provide accurate winds in storms with large spatial coverage. SMAP's wide swath wind field measurements enable it to give the expected R34 estimates. However, due to the coarse spatial resolution of SMAP, the impact of spatial averaging reduces the maximum wind speed in the TC eyewall region and can possibly lead to underestimates in intensity [e.g., Fig. 6(b)]. Compared with SMAP, the *C*-band SARs have much higher resolution, are able to resolve TC eye features, and exhibit the fine-scale characteristics of the TC wind field. For Typhoon Lionrock, the SAR-derived maximum wind speed estimates are closer to the best-track data than those of SMAP. It is also important to point out that heavy rainfall under extreme weather conditions attenuate *C*-band radar signals and, thus, impact the accuracy of retrieved high wind speeds [27], [37]–[41]. Moreover, the SAR swath is smaller than that of SMAP, which can possibly cause notable differences in R34 estimates between the SAR and best-track data. Thus, the complementarity of SMAP and SAR is valuable in order to obtain the reasonable measurements of TC surface wind structure and intensity.

SMAP and SAR multitemporal wind fields clearly show the evolution and intensity change process for Typhoon Noru. SAR-derived high-resolution wind fields illustrate the fine-scale features of Noru. SMAP-estimated R34 values are in good agreement with the best-track report. Note that SMAP cannot resolve the location of the eye due to its coarse resolution, particularly when Noru becomes very strong. During the lifecycle of Noru, SAR and SMAP both show symmetric and asymmetric characteristics of the wind field, e.g., depending on when Noru is strong or weak. Moreover, SMAP- and SAR-derived maximum wind speeds display similar trends in intensity variation with the best-track data. In this study, we demonstrate that synergistic wind observations of passive radiometer and active SAR instruments provide a good opportunity for monitoring the variability of TC intensity and surface wind structure. In the future, uncertainty regarding the availability of the best-track data can potentially be reduced by incorporating radiometer and

SAR TC observations into monitoring and forecasting programs. Moreover, satellite-derived surface wind structure and intensity parameters may help to find correct initial storm wind estimates and, thus, improve forecast skill for TC track and intensity. TC surface winds from multimission satellites also have the capability to provide realistic atmospheric forcing for ocean models, which have the potential to enhance the model simulations of upper ocean responses to TCs.

ACKNOWLEDGMENT

The authors would like to thank the Canadian Space Agency and European Space Agency for providing RADARSAT-2 and Sentinel-1A/B SAR data, and anonymous reviewers for their insightful suggestions and constructive comments. The views, opinions, and findings contained in this article are those of the authors personally and do not reflect any positions, policies, or decisions of Canada, U.S., and China government and agencies.

REFERENCES

[1] C. R. Sampson *et al.*, "Objective guidance for use in setting tropical cyclone conditions of readiness," *Weather Forecasting*, vol. 27, no. 4, pp. 1052–1060, 2012.

[2] M. DeMaria *et al.*, "Improvements to the operational tropical cyclone wind speed probability model," *Weather Forecasting*, vol. 28, no. 3, pp. 586–602, 2013.

[3] M. A. Bender, T. P. Marchok, C. R. Sampson, J. A. Knaff, and M. J. Morin, "Impact of storm size on prediction of storm track and intensity using the 2016 operational GFDL hurricane model," *Weather Forecasting*, vol. 32, no. 4, pp. 1491–1508, 2017.

[4] B. A. Harper, J. D. Kepert, and J. D. Ginger, "Guidelines for converting between various wind averaging periods in tropical cyclone conditions," World Meteorol. Org., Geneva, Switzerland, Tech. Rep. WMO/TD-1555, 2010.

[5] M. D. Powell and T. A. Reinhold, "Tropical cyclone destructive potential by integrated kinetic energy," *Bull. Amer. Meteorol. Soc.*, vol. 88, no. 4, pp. 513–526, 2007.

[6] V. F. Dvorak, "Tropical cyclone intensity analysis and forecasting from satellite imagery," *Monthly Weather Rev.*, vol. 103, no. 5, pp. 420–430, 1975.

[7] C. S. Velden, T. L. Olander, and R. M. Zehr, "Development of an objective scheme to estimate tropical cyclone intensity from digital geostationary satellite imagery," *Weather Forecasting*, vol. 13, no. 1, pp. 172–186, 1998.

[8] T. L. Olander and C. S. Velden, "The advanced Dvorak technique: Continued development of an objective scheme to estimate tropical cyclone intensity using geostationary infrared satellite imagery," *Weather Forecasting*, vol. 22, no. 2, pp. 287–298, 2007.

[9] K. Dolling, E. A. Ritchie, and J. S. Tyo, "The use of the deviation angle variance technique on geostationary satellite imagery to estimate tropical cyclone size parameters," *Weather Forecasting*, vol. 31, no. 5, pp. 1625–1642, 2016.

[10] J. A. Knaff, C. J. Slocum, K. D. Musgrave, C. R. Sampson, and B. R. Strahl, "Using routinely available information to estimate tropical cyclone wind structure," *Monthly Weather Rev.*, vol. 144, no. 4, pp. 1233–1247, 2016.

[11] J. L. Demuth, M. DeMaria, J. A. Knaff, and T. H. Vonder Harr, "Evaluation of advanced microwave sounding unit tropical cyclone intensity and size estimation algorithms," *J. Appl. Meteorol. Climatol.*, vol. 43, no. 2, pp. 282–296, 2004.

[12] M. Morris and C. S. Ruf, "Determing tropical cyclone surface wind speed structure and intensity with the CYGNSS satellite constellation," *J. Appl. Meteorol. Climatol.*, vol. 56, no. 7, pp. 1847–1865, 2017.

[13] M. J. Brennan, C. C. Hennon, and R. D. Knabb, "The operational use of QuikSCAT ocean surface vector winds at the National Hurricane Center," *Weather Forecasting*, vol. 24, no. 3, pp. 621–645, 2009.

[14] D. R. Chavas and K. A. Emanuel, "A QuikSCAT climatology of tropical cyclone size," *Geophys. Res. Lett.*, vol. 37, no. 18, 2010, Art. no. L18816, doi: 10.1029/2010GL044558.

[15] K. T. F. Chan and J. C. L. Chan, "Size and strength of tropical cyclones as inferred from QuikSCAT data," *Monthly Weather Rev.*, vol. 140, no. 3, pp. 811–824, 2012.

[16] C. R. Sampson, E. M. Fukada, J. A. Knaff, M. J. Brennan, B. R. Strahl, and T. Marchok, "Tropical cyclone gale wind radii estimates for the western North Pacific," *Weather Forecasting*, vol. 32, no. 3, pp. 1029–1040, 2017.

[17] N. Reul, J. Tenerelli, B. Chapron, D. Vandemark, Y. Quilfen, and Y. Kerr, "SMOS L-band radiometer: A new capability for ocean surface remote sensing in hurricanes," *J. Geophys. Res.*, vol. 117, no. C2, 2012, Art. no. C02006, doi: 10.1029/2011JC00747.

[18] S. H. Yueh *et al.*, "SMAP L-band passive microwave observations of ocean surface wind during severe storms," *IEEE Trans. Geosci. Remote Sens.*, vol. 54, no. 12, pp. 7339–7350, Dec. 2016.

[19] T. Meissner, L. Ricciardulli, and F. J. Wentz, "Capability of the SMAP mission to measure ocean surface winds in storms," *Bull. Amer. Meteorol. Soc.*, vol. 98, no. 8, pp. 1660–1677, 2017.

[20] N. Reul *et al.*, "A new generation of tropical cyclone size measurements from space," *Bull. Amer. Meteorol. Soc.*, vol. 98, no. 11, pp. 2367–2385, 2017.

[21] A. G. Fore, S. H. Yueh, B. W. Stiles, W. Tang, and A. K. Hayashi, "SMAP radiometer-only tropical cyclone intensity and size validation," *IEEE Geosci. Remote Sens. Lett.*, vol. 15, no. 10, pp. 1480–1484, Oct. 2018.

[22] Z. Sun, B. Zhang, W. Perrie, and J. A. Zhang, "Examination of surface wind asymmetry in tropical cyclones over the northwest Pacific ocean using SMAP observation," *Remote Sens.*, vol. 11, no. 22, 2019, Art. no. 2604.

[23] B. Zhang and W. Perrie, "Cross-polarized synthetic aperture radar: A new potential measurement technique for hurricanes," *Bull. Amer. Meteorol. Soc.*, vol. 93, no. 4, pp. 531–541, 2012.

[24] B. Zhang, W. Perrie, J. A. Zhang, E. W. Uhlhorn, and Y. He, "High-resolution hurricane vector winds from C-band dual-polarization SAR observations," *J. Atmos. Ocean. Technol.*, vol. 31, no. 2, pp. 272–286, 2014.

[25] A. A. Mouche, B. Chapron, B. Zhang, and R. Husson, "Combined co- and cross-polarized SAR measurements under extreme wind conditions," *IEEE Trans. Geosci. Remote Sens.*, vol. 55, no. 12, pp. 6746–6755, Dec. 2017.

[26] S. Fan, B. Zhang, A. A. Mouche, W. Perrie, J. A. Zhang, and G. Zhang, "Estimation of wind direction in tropical cyclones using C-band dual-polarization synthetic aperture radar," *IEEE Trans. Geosci. Remote Sens.*, vol. 58, no. 2, pp. 1450–1462, Feb. 2020.

[27] A. Mouche, B. Chapron, J. Knaff, Y. Zhao, B. Zhang, and C. Combot, "Copolarized and cross-polarized SAR measurements for high-resolution description of major hurricane wind structures: Application to Irma category 5 hurricanes," *J. Geophys. Res.*, vol. 124, no. 6, pp. 3905–3922, 2019.

[28] G. Zhang, W. Perrie, B. Zhang, J. Yang, and Y. He, "Monitoring of tropical cyclone structures in ten years of RADARSAT-2 SAR images," *Remote Sens. Environ.*, vol. 236, 2020, Art. no. 111449.

[29] K. R. Knapp, M. C. Kruk, D. H. Levinson, H. J. Diamond, and C. J. Neumann, "The international best track archive for climate stewardship (IBTrACS) unifying tropical cyclone data," *Bull. Amer. Meteorol. Soc.*, vol. 91, no. 3, pp. 363–376, 2010.

[30] C. J. McAdie and M. B. Lawrence, "Improvements in tropical cyclone track forecasting in the Atlantic basin, 1970–98," *Bull. Amer. Meteorol. Soc.*, vol. 81, no. 5, pp. 989–998, 2000.

[31] C. M. Kishtawal, N. Jaiswal, R. Singh, and D. Niyogi, "Tropical cyclone intensification trends during satellite era (1986-2010)," *Geophys. Res. Lett.*, vol. 39, no. 10, 2012, Art. no. L10810, doi: 10.1029/2012GL051700.

[32] K. T. Bhatia *et al.*, "Recent increases in tropical cyclone intensification rates," *Nature Commun.*, vol. 10, 2019, Art. no. 635.

[33] J. P. Kossin, "A global slowdown of tropical-cyclone translation speed," *Nature*, vol. 558, pp. 104–107, 2018.

[34] S. Wang, T. Rashid, H. Throp, and R. Toumi, "A shortening of the life cycle of major tropical cyclones," *Geophys. Res. Lett.*, vol. 47, no. 14, 2020, Art. no. e2020GL088589.

[35] C. W. Landsea and J. L. Franklin, "Atlantic hurricane database uncertainty and presentation of a new database format," *Monthly Weather Rev.*, vol. 141, no. 10, pp. 3576–3592, 2013.

[36] R. D. Torn and C. Snyder, "Uncertainty of tropical cyclone best-track information," *Weather Forecasting*, vol. 27, no. 3, pp. 715–729, 2012.

[37] A. Reppucci, S. Lehner, J. Schulz-Stellenfleth, and C. S. Yang, "Extreme wind conditions observed by satellite synthetic aperture radar in the North West Pacific," *Int. J. Remote Sens.*, vol. 29, no. 21, pp. 6129–6144, 2008.

[38] G. Zhang, X. Li, W. Perrie, B. Zhang, and L. Wang, "Rain effects on the hurricane observations over the ocean by C-band synthetic aperture radar," *J. Geophys. Res. Oceans*, vol. 121, pp. 14–26, 2016, doi: 10.1002/2015JC011044.

[39] B. Zhang and W. Perrie, "Recent progress on high wind speed retrieval from multi-polarization SAR imagery: A review," *Int. J. Remote Sens.*, vol. 35, no. 11/12, pp. 4031–4045, 2014, doi: 10.1080/01431161.2014.916451.

[40] W. Alpers, B. Zhang, A. Mouche, K. Zeng, and P. W. Chan, "Rain footprints on C-band synthetic aperture radar images of the ocean—Revisited," *Remote Sens. Environ.*, vol. 187, pp. 169–185, 2016.

[41] B. Zhang and W. Alpers, "The effect of rain on radar backscattering from the ocean," in *Advance in SAR Remote Sensing of Oceans*. Boca Raton, FL, USA: CRC Press, 2018, pp. 317–330.

Biao Zhang (Senior Member, IEEE) received the B.S. degree in surveying and mapping engineering from the China University of Petroleum, Dongying, China, in 2003, and the Ph.D. degree in physical oceanography from the Institute of Oceanology, Chinese Academy of Sciences, Qingdao, China, in 2008.

From 2008 to 2011, he was with the Bedford Institute of Oceanography, Canada, where he was a Postdoctoral Fellow and involved in developing synthetic aperture radar ocean surface wave and wind retrieval algorithms and products. He is currently a Professor with the School of Marine Sciences, Nanjing University of Information Science and Technology, Nanjing, China. His research interests include satellite remote sensing of marine dynamic environment and tropical cyclone, air–sea interaction under extreme weather conditions, Arctic sea ice monitoring by active and passive microwave sensors, and radar constellation mission.

Dr. Zhang was a recipient of the Visiting Fellow Scholarship of Natural Sciences and Engineering Research Council of Canada, the first award of Science and Technology from Jiangsu Province in 2017 and Ocean Science and Technology from the State Oceanic Administration of China, the second award of Natural Science from the Ministry of Education of China in 2014, and the Outstanding Young Scientist Award by the National Science Foundation of China in 2016. He was selected "Six Talent Peaks" of Jiangsu Province in 2018.

Ziqiang Zhu received the B.S. degree in marine science in 2018 from the School of Marine Science, Nanjing University of Information Science and Technology, Nanjing, China, where he is currently working toward the M.S. degree in marine meteorology.

His research interests include remote sensing of tropical cyclone (TC) intensity and structure, and develop parameterized TC surface wind model.

William Perrie received the B.S. degree in physics from the University of Toronto, Toronto, ON, Canada, in 1973, and the Ph.D. degree in meteorology and oceanography from the Massachusetts Institute of Technology, Cambridge, MA, USA, in 1979.

He was a Postdoctoral Fellow in oceanography and mathematics with the University of British Columbia, Vancouver, BC, Canada, and the National Center for Atmospheric Research, Boulder, CO, USA. He is currently a Senior Scientist with the Bedford Institute of Oceanography, Dartmouth, NS, Canada, and an Adjunct Professor with Dalhousie University, Halifax, NS, Canada. His research interests include the modeling of ocean waves, air–sea fluxes, coupled atmosphere–ocean interactions and impacts of climate change on these variables, and field measurements via remote sensing and *in situ* of winds, waves, and currents.

Jie Tang received the B.S. and Ph.D. degrees in atmospheric science from Nanjing University, Nanjing, China, in 2001 and 2006, respectively.

In 2014 and 2015, he was a Visiting Scientist with National Oceanic and Atmospheric Administration/Atlantic Oceanographic and Meteorological Laboratory, and a visiting scholar with the Ludwig Maximilian University of Munich, Germany. He is currently a Research Fellow with Shanghai Typhoon Institute, China Meteorological Administration (CMA), Beijing, China. His research interests include tropical cyclone boundary layer, extratropical transition, typhoon forecast techniques, and typhoon field campaign.

Dr. Tang was a recipient of the Excellent Young Meteorological Scientist of CMA, and Technology Advance Award of Shanghai City. He has been the Chairperson of the Working Group of Meteorology, World Meteorological Organization/Economic and Social Commission for Asia, and the Pacific Typhoon Committee, since 2021.

Jun A. Zhang (Senior Member, IEEE) received the B.S. degree in naval architecture and ocean engineering from the Dalian University of Technology, Dalian, China, in 2000, and the Ph.D. degree in applied marine physics from the Rosenstiel School of Marine and Atmospheric Science, University of Miami, Miami, FL, USA, in 2007.

He was a Postdoctoral Fellow with National Research Council. He is currently a Scientist with Hurricane Research Division/Atlantic Oceanographic and Meteorological Laboratory/National Oceanic and Atmospheric Administration, Washington, DC, USA, and University of Miami, Miami, FL, USA. His research interests include boundary layer structure and dynamics, turbulence, air–sea interaction, remote sensing, and physical parameterizations.

Dr. Zhang was a recipient of Cooperative Institute for Marine and Atmospheric Studies Gold Medal Award in recognition of his role in improving the operational hurricane weather research and forecasting model, American Meteorological Society's Banner I. Miller Award, National Aeronautics and Space Administration Award for Hurricane and Severe Storm Sentinel Group Achievement, and Aviation Laureate Award. He has been the Chief Editor for the *Dynamics of Atmospheres and Oceans*, since 2019.